

# Analytic Modeling of Exciton Decay Dynamics to Extract Intrinsic Single Walled Carbon Nanotube Properties

Mitchell D. Anderson,<sup>\*</sup> Yee-fang Xiao, and James M. Fraser<sup>\*</sup>

*Department of Physics, Engineering Physics & Astronomy, Queen's University, Kingston,  
Ontario, K7L 3N6 Canada*

E-mail: manderson@physics.queensu.ca; fraser@physics.queensu.ca

## Abstract

The quantum yield of semiconducting single walled carbon nanotubes is limited by strong diffusion driven end/defect quenching and rapid Auger-like exciton-exciton annihilation (EEA) processes. While these two processes have been extensively studied independently, we show that both effects must be considered to properly extract intrinsic nanotube properties. To achieve this result, we have developed a convenient analytic model of exciton dynamics (verified by comparison to Monte Carlo simulations) that shows the *intrinsic* optical quantum efficiency is substantially higher than previously reported from observations in typical samples. Diffusion limited EEA is modeled using a one dimensional line segment revealing enhanced annihilation at low exciton populations. Lastly, the analytic model is demonstrated using non-linear EEA effects to extract intrinsic absorption cross sections, lifetimes, and diffusion lengths for SWCNTs.

---

<sup>\*</sup>To whom correspondence should be addressed

# Introduction

Many interesting photo-physical applications utilizing single walled carbon nanotubes (SWCNTs) are emerging that take advantage of two dominant non-radiative decay pathways, end/defect quenching and rapid Auger like exciton-exciton annihilation (EEA).<sup>1</sup> At low exciton densities, the stochastic fluctuations of the optical emission intensity due to adsorption and desorption of fluorescence quenchers has led to single molecule counting arrays and biological sensors.<sup>2-5</sup> At high exciton densities, the rapid relaxation of excitons has been useful in creating saturable absorbers for passive mode-locking<sup>6-9</sup> and may give rise to photon anti-bunching,<sup>10</sup> showing promise for single photon sources with selectable wavelengths from optical frequencies into the telecom band.

Following the work of Cognet and Weisemann, first demonstrating stochastic quenching of excitons in SWCNTs,<sup>11</sup> much effort has gone into modeling the length and defect dependent quantum efficiency and exciton lifetimes.<sup>12-17</sup> These models have been developed ignoring EEA since it was expected that at low excitation fluences non-radiative decay would be dominated by end/defect quenching.<sup>12</sup> However, the fluence at which EEA plays a role is surprisingly low, as has been observed by nonlinear photoluminescence (PL) effects for both continuous wave (CW)<sup>18,19</sup> and pulsed<sup>20,21</sup> laser excitation, putting into question whether EEA can be ignored for low to moderate fluences.

It is clear that as the excitation fluence is increased, EEA dominates the exciton decay dynamics and substantially reduces the optical quantum efficiency. The rapid injection of many excitons under pulsed excitation leads to a complete saturation of the SWCNT photoluminescence<sup>20,21</sup> while even under CW excitation a strong nonlinearity has been observed at surprisingly low fluences<sup>18,19</sup> and was proposed to be an effect of long lived optical quenchers.<sup>19</sup> For both pulsed and CW excitation, the nonlinear fluence dependence of the photoluminescence has been modeled as a diffusion limited process.<sup>19,22,23</sup> However, a full microscopic model of exciton dynamics which properly accounts for the spatial and density dependence of exciton lifetime is still absent. In fact, the existing analytic diffusion limited EEA model<sup>23</sup> approximates a SWCNT as a ring which leads to an incor-

rect exciton pair distribution function, overestimating the exciton separation and underestimating EEA at low exciton levels. In this work we consider three competing decay processes, linear decay ( $P_T$ ), decay due to exciton-exciton annihilation ( $P_{EEA}$ ), and decay due to end quenching ( $P_{END}$ ). This microscopic model can be used to accurately determine *intrinsic* SWCNT properties such as the optical absorption, quantum efficiency, exciton lifetime, and diffusion length for any SWCNT sample.

## Results and discussion

### Exciton End Quenching

While the study of exciton diffusion limited quenching at SWCNT ends and defect sites has been explored extensively,<sup>13,15–18</sup> it has not been developed considering many body exciton-exciton annihilation and does not properly account for the spatial dependence of the effective exciton lifetime. For this reason, the following diffusion-end quenching formalism is developed which can be easily incorporated into a diffusion limited EEA model. An exciton can be treated diffusively and not ballistically as long as,  $L \gg \sqrt{2D_X\Delta t}$ , where  $L$  is the nanotube length,  $D_X$  is the diffusion constant, and  $\Delta t$  is the scattering time and is approximately equal to the dephasing time  $T_2$ .<sup>16</sup> In this case, the diffusion of an exciton in one dimension obeys the diffusion equation  $\delta_t n(x, t) = D_X \delta_x^2 n(x, t)$ . If the SWCNT ends quench with a probability of 1, then the probability that an exciton created at a position  $x$  on a line segment  $[0, L]$  will survive after time  $t$  is equal to the probability that it has not passed through the positions a distance  $x$  or  $L - x$  away. From the first passage time of a Brownian motion,<sup>24</sup> the probability that an exciton, starting at position 0, has not passed a position a distance  $x$  away after time  $t$  is,

$$P(x, t) = \text{erf}\left(\frac{1}{2} \frac{x}{\sqrt{D_X t}}\right) \quad (1)$$

where  $\text{erf}(z) = (2/\sqrt{\pi}) \int_0^z e^{-t^2} dt$  is the error function.

For a SWCNT of length  $L$  with only the two ends as quenching sites, such as suspended from a trench, the average probability that an exciton survives after time  $t$  is,

$$P_{END}(L, t) = \frac{\int_0^L g(x)P(x, t)P(L-x, t)dx}{\int_0^L g(x)dx} \quad (2)$$

where  $g(x)$  is the spatial weighting function determined by the excitation source. In the case of homogeneous excitation,  $g(x) = 1$  resulting in,

$$P_{END}(\tau_D, t) = \left[ \text{erf} \left( \frac{1}{2} \sqrt{\frac{\tau_D}{2t}} \right) \right]^2 - \sqrt{\frac{32t}{\pi\tau_D}} \left[ \frac{1}{\sqrt{2}} \text{erf} \left( \sqrt{\frac{\tau_D}{4t}} \right) - \text{erf} \left( \sqrt{\frac{\tau_D}{8t}} \right) e^{-\frac{\tau_D}{8t}} \right] \quad (3)$$

where  $\tau_D = L^2/D_X$  is the only physical parameter and is essentially the average “diffusional time”.<sup>23</sup> In the limit that  $t \ll \tau_D$  Eq. (3) simplifies to  $P_{END}(\tau_D, t) \approx 1 - 4\sqrt{t/\pi\tau_D}$  but in general calculations are not done in this limit since we are interested in both short and long time dynamics. The exciton population decay due to end effects [Eq. (3)] is shown in Figure 1(a) for several values of  $\tau_D$ . It is useful to note that the exciton population decay to the edges without intrinsic decay is on time scales comparable to those measured in PL lifetime measurements.<sup>25</sup> In general, because of the spatial dependence of the exciton population decay, this is not equivalent to a Poissonian decay with an effective decay rate  $\Gamma_{eff}$ , as has commonly been modeled.

In addition to non-radiative end quenching excitons also undergo linear radiative and non-radiative decay with the survival probability  $P_\Gamma(t) = e^{-\Gamma t}$ . Here  $\Gamma = \Gamma_R + \Gamma_{NR}$  is the linear decay rate from radiative ( $\Gamma_R$ ) and non-radiative ( $\Gamma_{NR}$ ) linear decay. End quenching is taken to be independent of linear decay so the survival probabilities can be multiplied and the exciton decay dynamics follow,  $P(\tau_D, t) = P_{END}(\tau_D, t) \times P_\Gamma(t)$ . To determine the quantum efficiency ( $\eta_{QE}$ ) of a system for which the exciton population decay follows an arbitrary function, we note that the probability of radiative decay in an infinitesimal time  $dt$  is  $\Gamma_R dt$ . It follows that the number of excitons that radiatively decay at time  $t$  is simply the probability of radiative decay times the total number

of excitons at time  $t$ ,  $N_{rad}(t) = N_{ex}(t)\Gamma_R dt$  where  $N_{ex}(t) = N_0 P(t)$  starting with the injected exciton number  $N_0$ . The total number of excitons that radiatively decay is then  $N_{rad} = N_0 \Gamma_R \int_0^\infty P(t) dt$ , allowing the quantum efficiency can be written as,

$$\eta_{QE} = \frac{N_{rad}}{N_0} = \Gamma_R \int_0^\infty P(t) dt \quad (4)$$

for any arbitrary decay function  $P(t)$ . In the simple case where end effects are negligible (for example  $L \rightarrow \infty$ )  $P_{END}(\infty, t) \rightarrow 1$  and the exciton population decay ( $P_T \times P_{END}$ ) simplifies to a standard mono-exponential decay,<sup>26</sup>  $P(t) = e^{-\Gamma t}$ , and the solution to Eq. (4) is the intrinsic quantum efficiency  $\eta_0 = \Gamma_R/\Gamma$ .

Typical SWCNT lengths range from  $\sim 100$  nm to  $> 50 \mu\text{m}$ <sup>17,27</sup> and diffusivities range from  $\sim 0.1 - 100 \text{ cm}^2/\text{s}$ .<sup>11,18,28,29</sup> Within this typical range, there is over an order of magnitude decrease in the optical quantum efficiency compared to the intrinsic quantum efficiency due to end quenching as can be seen in Figure 1(b). As verification, the analytic model is compared to standard Monte Carlo simulations [see Methods], which are processor and time intensive and are of limited value in identifying the importance of the underlying microscopic processes. The effect of a SWCNT ensemble with random defect sites can easily be calculated by averaging over the permutations of smaller effective lengths.

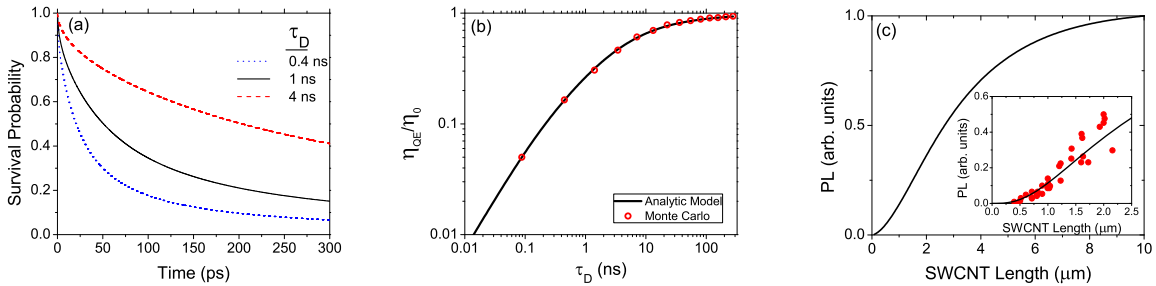


Figure 1: (a) Exciton survival probability ( $P_{END}$ ) due to end quenching [Eq. (3)] for several values of the average diffusional time  $\tau_D$ . (b) Quantum efficiency [Eq. (4)] as a function of the average diffusional time ( $\tau_D$ ) with  $\Gamma = 3.3 \text{ ns}^{-1}$ . (c) Photoluminescence from “pristine” SWCNTs ( $\Gamma = 3.3 \text{ ns}^{-1}$  and  $D_X = 44 \text{ cm}^2/\text{s}$ ) of various lengths excited with a Gaussian beam ( $\sigma = 520 \text{ nm}$ ) and [INSET] compared to experimental data collected by Moritsubo *et al.*<sup>18</sup>

As an example of the utility of this formalism, the photoluminescence dependence on tube length can be calculated since  $PL \propto \eta_{QE}$ , shown in Figure 1(c). This can be compared to experimental results collected for variable tube lengths (such as done by Moritsubo *et al.*<sup>18</sup>), shown in Figure 1(c) [INSET], and can be used to extract intrinsic properties. Experimental studies use Gaussian beam excitation ( $\sigma = 520$  nm) which are included using Eq. (2) with  $g(x) = \exp(-(x - L/2)^2/\sigma^2)$ . The measured 8 meV linewidth corresponds to a room temperature thermal diffusivity of  $D_X = 44$  cm<sup>2</sup>/s.<sup>16</sup> It should be noted that in general, intrinsic lifetimes (i.e.,  $\tau = 1/\Gamma$ ) is difficult to directly obtain from experimental time-resolved population measurements, since such studies measure effective lifetimes which include quenching at ends. Moritsubo *et al.* use 85 ps effective lifetimes based on single SWCNT femtosecond excitation correlation (FEC) measurements.<sup>21</sup> Analysis of the original FEC data using the model outlined in this manuscript, extracts an intrinsic effective lifetime around four times longer than the effective value ( $\tau = 1/\Gamma = 300$  ps). With one additional fit parameter (for y-scaling), the analytic model prediction shows good agreement with experimental observations (Figure 1(c) [INSET]). Longer SWCNT lengths would further constrain parameter fitting.

The intrinsic exciton diffusion length  $\sqrt{D_X \tau}$  is found here to be  $\sim 1.2$   $\mu$ m. For finite length SWCNTs, the observed diffusion length is shorter since the effective lifetime is shortened by end effects. Though this analysis allows extraction of certain SWCNT parameters such as diffusion length, results are still linearly dependent on exciton number and therefore cannot decouple the PL action cross section ( $PLAC = \eta_{QE} \times \sigma_{ab}$ ) to extract the quantum efficiency ( $\eta_{QE}$ ) and the optical absorption cross section ( $\sigma_{ab}$ ). To do this, experimental results at higher fluences involving exciton-exciton annihilation are required.

## Exciton-Exciton Annihilation

As the excitation fluence is increased, for both CW<sup>18,19</sup> and pulsed<sup>20,21</sup> excitation, EEA substantially reduces the optical quantum efficiency. Even with average exciton densities less than one exciton injected for every diffusion length, we show that diffusion mediated annihilation can oc-

cur.

Previous work on exciton diffusion-reaction modeling<sup>23</sup> in carbon nanotubes used the geometry of a one dimensional ring<sup>30</sup> which is a good approximation for infinitely long SWCNTs and/or large exciton densities, but is not in general correct. In many SWCNT samples the ratio of diffusion length to tube length can be quite high<sup>13,15–18</sup> and PL saturation has been observed even for quite low exciton densities making this regime important to model correctly.<sup>21</sup> The assertion that the pair distribution function for the ring model is not appropriate can be easily understood from a two exciton example; in a ring geometry all possible initial pair separation lengths are equally likely<sup>30</sup> while for a line segment there are many ways to place an exciton pair separated by a few nanometers but there is only one way to place two excitons the length of the nanotube apart. Since, the excitons on average will be farther apart for the ring pair distribution function, application of this model will underestimate the role of EEA. To model the dynamics on a finite line segment, the pair distribution function for  $N$  particles is,<sup>31</sup>

$$\begin{aligned} f(L_X, N) dL_X &= \frac{N}{L(1-\theta)} \left[ 1 - \frac{L_X - R}{L(1-\theta)} \right]^{N-1} dL_X \\ &\approx \frac{N}{L^N} (L - L_X)^{N-1} dL_X, \quad R \rightarrow 0 \end{aligned} \quad (5)$$

where  $L$  is the SWCNT length,  $R$  is the exciton size,  $L_X$  is the nearest neighbor exciton separation, and  $\theta = NR/L$ . In this work, we treat the exciton as a point particle ( $R \rightarrow 0$ ) which simplifies Eq. (5). As a simple example of the difference between ring and line models, the pair distribution function for a line has a mean separation of  $L/(N+1)$  and not  $L/N$  as expected for a ring.<sup>23</sup> In the thermodynamic limit the pair distribution functions converge, but for low exciton densities, the focus of this work, the geometrical distinction is significant and the annihilation dynamics are different.

Before expanding into the  $N$  exciton case, we first consider the simple case of two excitons with an initial separation  $L_X$  independently undergoing one dimensional diffusion. In this model two excitons are taken to annihilate if they spatially overlap in their lifetime, resulting in one exciton

being destroyed and the other promoting to a higher energy state from which it quickly relaxes back into a thermal  $E_{11}$  state. Similar to a single exciton undergoing diffusion to a stationary quenching site (Eq. (1)), the probability that the separation (initially  $L_X$ ) of two excitons undergoing relative diffusion has not reached 0 after time  $t$  can be written as,  $\text{erf}(L_X/(2\sqrt{2D_Xt}))$ . This is equivalent to a single exciton diffusing with diffusion constant  $2D_X$ . Therefore the average probability that an exciton pair has not undergone EEA after time  $t$  is the mean of survival probabilities weighted with the pair distribution function (Eq. (5)):

$$P_{EEA}^{sur}(N, L, D_X, t) = \int_0^L f(L_X, N) \text{erf}\left(\frac{1}{2} \frac{L_X}{\sqrt{2D_Xt}}\right) dL_X \quad (6)$$

For the case of  $N = 2$ , this simplifies to,

$$P_{EEA}^{sur}(2, \tau_D, t) = \left(\frac{4}{\tau_D}t + 1\right) \text{erf}\left(\frac{1}{4}\sqrt{\frac{2\tau_D}{t}}\right) - 4\sqrt{\frac{2t}{\pi\tau_D}} \left(1 - \frac{1}{2}e^{-\frac{1}{8}\frac{\tau_D}{t}}\right) \quad (7)$$

where again, the only physical parameter is  $\tau_D$ , the average diffusional time. This contrasts with the ring model which for two particle EEA predicts,  $P_{EEA}^{sur}(2, \tau_D, t) = \text{erf}\left(\sqrt{\tau_D/32t}\right)$ .<sup>23</sup> In Figure 2, the results of the two models (for  $\tau_D = 5.7$  ns) are compared to Monte Carlo simulations for exciton dynamics in a finite length SWCNT. It can be seen that for the two exciton case the exciton pair survivability for typical exciton lifetime ( $\sim 50$ -300 ps) is reduced by  $\sim 30\%$  compared to predictions from previous work.

Using the exciton pair survivability (Eq. (6)), the total number of excitons that survive EEA after time  $t$ , can be written as  $(1 + (N - 1)P_{EEA}^{sur}(N, \tau_D, t))$ , which has been verified by Monte Carlo simulations. This assumes one exciton of the pair survives EEA. The solution for this is the generalized hypergeometric function,



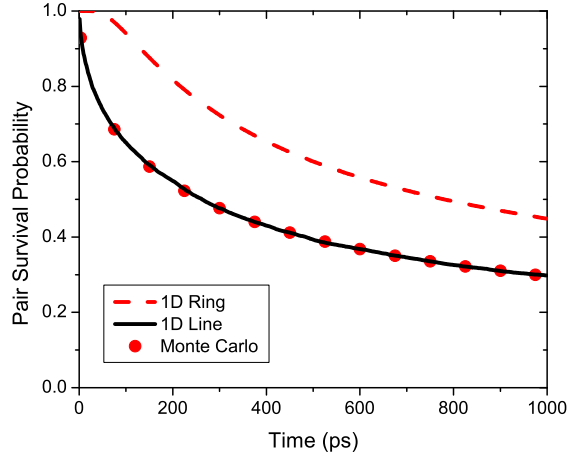


Figure 2: Analytic solutions for the EEA pair survival probability for a ring<sup>23</sup> and line segment for a 5  $\mu\text{m}$  SWCNT with  $D_X = 44 \text{ cm}^2/\text{s}$  compared to Monte Carlo simulations.

$$N_{ex}(N, \tau_D, t) = 1 + \frac{N-1}{N+1} \left( \sqrt{\frac{\tau_D}{2t}} \right) \frac{\Gamma(\frac{N}{2} + 1) \Gamma(\frac{N}{2} + \frac{3}{2})}{\pi} \times \left[ \sum_{k=0}^{\infty} \frac{(-\frac{\tau_D}{8t})^k}{k!} \frac{\Gamma(k+1) \Gamma(k + \frac{1}{2})}{\Gamma(k + \frac{N}{2} + 1) \Gamma(k + \frac{N}{2} + \frac{3}{2})} \right] \quad (8)$$

where  $\Gamma(x)$  is the Gamma function. From this it follows that, given  $N_0$  initial excitons, the probability an exciton survives EEA is simply  $P_{EEA}(N_0, \tau_D, t) = N_{ex}(N_0, \tau_D, t)/N_0$ . In the case of a single injected exciton, the survival probability  $P_{EEA}$  remains 1 for all times  $t$  as expected.

## Combined Exciton Decay Dynamics

Finally, to model the decay dynamics of the entire system including the three decay channels ( $P_\Gamma, P_{EEA}, P_{END}$ ), the exciton survival probabilities of the three decay channels are treated as independent so the total survival probability of the exciton population is simply,

$$P_{TOT}(N_0, \tau_D, \Gamma, t) = P_\Gamma(\Gamma, t) \times P_{END}(\tau_D, t) \times P_{EEA}(N_0, \tau_D, t) \quad (9)$$

This model ignores the interplay between  $P_{EEA}$  and both  $P_{END}$  and  $P_T$ , which slightly overestimates EEA and consequently underestimates the quantum efficiency compared to Monte Carlo simulations which do not rely on this approximation. Figure 3(a) shows an example of exciton dynamics from the analytic model compared to Monte Carlo simulations with increasing numbers of injected excitons for a 5  $\mu\text{m}$  long (9,8) SWCNT with diffusivity of 44  $\text{cm}^2/\text{s}$  and a linear relaxation rate  $\Gamma = 3.3 \text{ ns}^{-1}$  (*i.e.*,  $\tau_D = 5.7 \text{ ns}$ ), revealing good agreement. The quantum efficiency (Eq. (4)) for variable  $\tau_D$  can be calculated by Eq. (9) and agrees well with Monte Carlo simulations (Figure 3(b)). For a typical SWCNT, the effective quantum efficiency is significantly lower than the intrinsic quantum efficiency due to end quenching. The effective quantum efficiency is further reduced due to the highly efficient exciton-exciton annihilation, even for low exciton injection numbers (Figure 3(c)).

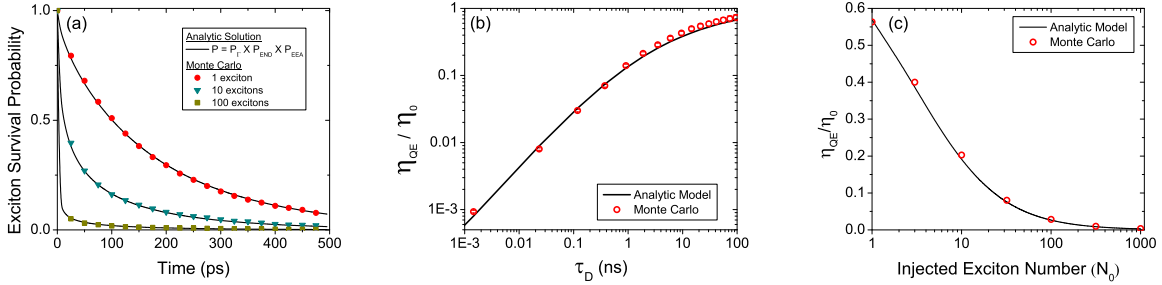


Figure 3: (a) The exciton survival probability (Eq. (9)) for 1, 10, and 100 injected excitons on a 5  $\mu\text{m}$  SWCNT (diffusivity= 44  $\text{cm}^2/\text{s}$ , linear decay rate  $\Gamma = 3.3 \text{ ns}^{-1}$ ) (b) The normalized quantum efficiency as a function of the average diffusional time with  $\Gamma = 3.3 \text{ ns}^{-1}$  for ten injected excitons. (c) The normalized quantum efficiency as a function of injected exciton number for  $\tau_D = 5.7 \text{ ns}$  and  $\Gamma = 3.3 \text{ ns}^{-1}$  (corresponding to a 5  $\mu\text{m}$  SWCNT with a diffusivity of 44  $\text{cm}^2/\text{s}$ ).

The analytic analysis (Eq. (9)) recreates the order of magnitude difference in saturation density observed in photoluminescence studies between suspended and encapsulated samples<sup>20,21</sup> (Figure 4(a) where  $PL(N_0, \tau_D, \Gamma) = N_0 \eta_{QE}(N_0, \tau_D, \Gamma)$ ). The parameters used for encapsulated samples are;  $L = 610 \text{ nm}$ ,  $D_X = 4 \text{ cm}^2/\text{s}$ ,  $\Gamma = 50 \text{ ns}^{-1}$  and for air-suspended samples,  $L = 6 \mu\text{m}$ ,  $D_X = 44 \text{ cm}^2/\text{s}$ ,  $\Gamma = 3.3 \text{ ns}^{-1}$ . For comparison purposes, we define the saturation point ( $N_{sat}$ ) with a simple model where  $PL(N_0) \propto 1 - \exp(-N_0/N_{sat})$ . From Figure 4(a) it can be seen that, as experimentally observed, the injected exciton density at which photoluminescence saturation occurs in “pristine”

SWCNT samples is about an order of magnitude than in a bulk encapsulated sample. Any remaining discrepancies in the saturation fluence difference<sup>20,21</sup> is likely due to random SWCNT orientation relative to incident light polarization, nonuniform excitation intensity, random length distribution, and different optical absorptions of bulk samples.

As discussed earlier, even if the PL action cross-section is well quantified, it is challenging to decouple optical absorption from quantum efficiency. With fluences sufficiently high to cause exciton-exciton annihilation, the analytic model can be used to extract the optical absorption cross section ( $\sigma_{ab}$ ) for SWCNTs since it is directly linked to injected exciton number through the fluence,  $N_0 = N_c \times \sigma_{ab} \times Fluence$ , where  $N_c$  is the number of carbon atoms. For the most constrained results, independent measurements of the diffusivity (*e.g.*, from PL line width), length (*e.g.*, imaging), and decay lifetime (*e.g.*, femtosecond excitation correlation spectroscopy<sup>21,32</sup>), should be performed. As an example, Figure 4(b) shows a fit of the analytic model to experimental data for a single 4.6  $\mu\text{m}$  (9,8) air-suspended SWCNT [from Xiao et al.<sup>21</sup>]; the extracted absorption cross section is  $\sigma_{ab} = 5 \times 10^{-17} \text{ cm}^2/\text{atom}$ , which is about a factor of two higher than previously reported for SWCNTs on substrates.<sup>33</sup> Inputs to this model are the intrinsic linear lifetime of 218 ps (extracted from fitting the model to FEC data, see below) and a diffusivity of 44  $\text{cm}^2/\text{s}$ .<sup>18</sup>

The analytic model allows direct calculation of the underlying decay dynamics responsible for the sharp saturation in photoluminescence. For example, for each initial exciton number shown in Figure 4(c), the inset shows the corresponding normalized population decay dynamics compared to purely linear decay  $P_\Gamma$ . Increasing the injected exciton number significantly speeds up the population decay due to EEA, even at low injected exciton numbers.

This analytic model also shows good agreement with photoluminescence lifetime experiments and can be used to extract the intrinsic decay rate  $\Gamma$ , without the need for additional fit parameters provided by a phenomenological bi-exponential decay model.<sup>14</sup> An example of this is shown in Figure 4(d) where normalized femtosecond excitation correlation data [see Xiao et al.<sup>21</sup> for experimental details] is fit with the analytic model calculated for two injected pulses separated in time [see Supporting Information]. The complete model including end quenching and EEA shows

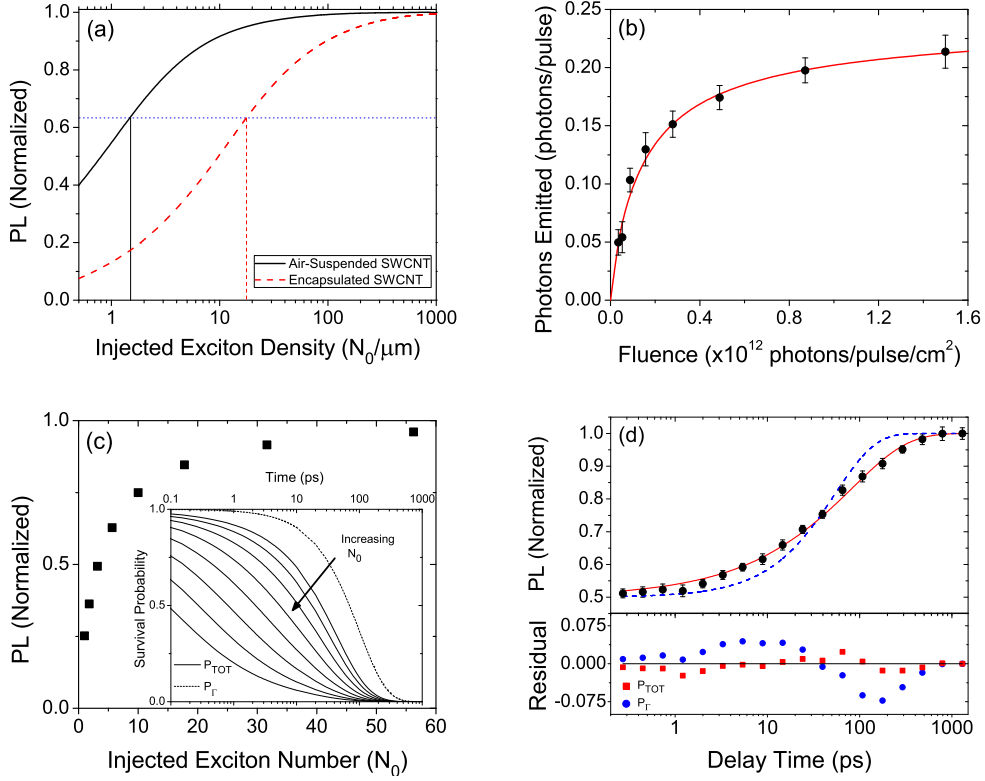


Figure 4: (a) Calculated photoluminescence for a typical encapsulated (red dashed curve) and air-suspended SWCNT (black solid curve) with the saturation point marked (as defined in text). (b) Analytic model (red curve), fit to experimental results (black circles) for a  $4.6 \mu\text{m}$  (9,8) air-suspended SWCNT. (c) [INSET] Exciton population decay dynamics as a function of injected exciton number with purely linear decay  $P_T$  for comparison. Each exciton decay curve corresponds to a point on the photoluminescence vs injected exciton number plot. (d) FEC data (black circles)<sup>21</sup> fit with model based on single exponential decay (blue dashed curve) and complete analytic model (red solid curve) and (bottom) corresponding residues.

better agreement to the data compared to simple linear decay. In both cases, only one fit parameter is used, namely  $\Gamma$ . Simple linear decay does not include end quenching, which is particularly relevant in the data for short time delays ( $<10$  ps), causing the linear relaxation process to appear faster than it is ( $18.5 \text{ ns}^{-1}$  for  $P_{\Gamma}$  compared to  $4.6 \text{ ns}^{-1}$  for  $P_{TOT}$ ). We anticipate that the model proposed here will be particularly useful to the effort in understanding the length dependence of exciton lifetimes<sup>14</sup> since it avoids additional fit parameters. Comparison of the models shows that when end quenching is ignored the intrinsic exciton lifetime, and consequently the intrinsic diffusion length, is significantly underestimated. Knowledge of a sample's intrinsic properties will allow for engineering of optoelectronic properties such as length or diffusivity to maximize the quantum efficiency (for optical emission applications) or decay rate (for applications requiring fast relaxation).

## Conclusion

In this work an analytic model of exciton decay dynamics and quantum efficiency is developed including the three dominant exciton decay channels, linear decay, end/defect quenching, and exciton-exciton annihilation. Results from this analytic model are verified with Monte Carlo simulations which require considerable processing time for convergence. The spatial dependence of the exciton lifetime due to diffusion assisted quenching is explicitly included removing the need for approximations and phenomenological parameters. Consequently this model correctly accounts for the length dependence of the exciton lifetime and can therefore be used with SWCNT length studies to extract *intrinsic* diffusion lengths or with exciton lifetime studies to extract *intrinsic* exciton decay rates.

In the multiple exciton regime, proper modeling of the exciton pair distribution function reveals that for realistic exciton densities, the commonly used one dimensional ring approximation significantly underestimates EEA. Modeling including EEA and end effects reveals a method of extracting the optical absorption cross section for SWCNTs using photoluminescence saturation

experiments where the injected exciton number is directly linked to the optical pump fluence. From this it is seen that occurrence of photoluminescence saturation at an order of magnitude different excitation fluence, as observed in past experiments with samples with different diffusional times and linear lifetimes, is reasonable when both end effects and EEA are accounted for.

## Methods

The Monte Carlo simulations are performed by considering a line segment of length  $L$ .  $N_0$  excitons are created at random positions along the interval  $[0, L]$  at time  $t = 0$ . For each time step  $\delta t$  each exciton takes a step of length  $\delta x = \sqrt{2D_X \delta t}$  in a random direction. Typically a value of  $\delta t = 50$  fs is used, however for small  $\tau_D$  a smaller  $\delta t$ , down below 1 fs, is used to achieve convergence. The probability that an exciton decays via a linear pathway for each temporal step is  $\Gamma \delta t \ll 1$ . If an exciton leaves the segment  $[0, L]$  it is destroyed. If two excitons spatially overlap, one is destroyed. Generally the results were averaged over  $> 50,000$  runs and each run continued until no excitons were left in the system. Numerical integration for the analytic model was performed using the Gauss-Kronrod quadrature method.

## Acknowledgement

We thank M. Abdelqader, C. Van Vlack and M. Dignam for helpful discussions. This work is funded by the Natural Sciences and Engineering Research Council of Canada, the Canadian Foundation for Innovation, and the Ministry of Research and Innovation (Ontario).

## Supporting Information Available

Supporting information is provided detailing theoretical analysis of femtosecond excitation correlation spectroscopy to fit normalized two pulse pump-pump experiments.

## References

1. Huang, L.; Krauss, T. Quantized Bimolecular Auger Recombination of Excitons in Single-Walled Carbon Nanotubes. *Phys. Rev. Lett.* **2006**, *96*, 57407.
2. Barone, P.; Baik, S.; Heller, D.; Strano, M. Near-Infrared Optical Sensors Based on Single-Walled Carbon Nanotubes. *Nat. Mater.* **2004**, *4*, 86–92.
3. Kim, J.; Heller, D.; Jin, H.; Barone, P.; Song, C.; Zhang, J.; Trudel, L.; Wogan, G.; Tannenbaum, S.; Strano, M. The Rational Design of Nitric Oxide Selectivity in Single-Walled Carbon Nanotube Near-Infrared Fluorescence Sensors for Biological Detection. *Nat. Chem.* **2009**, *1*, 473–481.
4. Ulissi, Z. W.; Zhang, J.; Boghossian, A. A.; Reuel, N. F.; Shimizu, S. F. E.; Braatz, R. D.; Strano, M. S. Applicability of Birth-Death Markov Modeling for Single-Molecule Counting Using Single-Walled Carbon Nanotube Fluorescent Sensor Arrays. *J. Phys. Chem. Lett.* **2011**, *2*, 1690–1694.
5. Boghossian, A.; Zhang, J.; Barone, P.; Reuel, N.; Kim, J.; Heller, D.; Ahn, J.; Hilmer, A.; Rwei, A.; Arkalgud, J. et al. Near-Infrared Fluorescent Sensors based on Single-Walled Carbon Nanotubes for Life Sciences Applications. *ChemSusChem* **2011**, *4*, 848–863.
6. Garnov, S.; Solokhin, S.; Obraztsova, E.; Lobach, A.; Obraztsov, P.; Chernov, A.; Bukin, V.; Sirotkin, A.; Zagumennyi, Y.; Zavartsev, Y. et al. Passive Mode-Locking with Carbon Nanotube Saturable Absorber in Nd: GdVO<sub>4</sub> and Nd: Y<sub>0.9</sub>Gd<sub>0.1</sub>VO<sub>4</sub> Lasers Operating at 1.34  $\mu\text{m}$ . *Laser Phys. Lett.* **2007**, *4*, 648–651.
7. Nicholson, J.; Windeler, R.; DiGiovanni, D. Optically Driven Deposition of Single-Walled Carbon-Nanotube Saturable Absorbers on Optical Fiber End-Faces. *Opt. Express* **2007**, *15*, 9176–9183.
8. Yim, J.; Cho, W.; Lee, S.; Ahn, Y.; Kim, K.; Lim, H.; Steinmeyer, G.; Petrov, V.; Griebner, U.;

- Rotermund, F. Fabrication and Characterization of Ultrafast Carbon Nanotube Saturable Absorbers for Solid-State Laser Mode Locking Near 1  $\mu\text{m}$ . *Appl. Phys. Lett.* **2008**, *93*, 161106.
9. Cho, W.; Schmidt, A.; Yim, J.; Choi, S.; Lee, S.; Rotermund, F.; Griebner, U.; Steinmeyer, G.; Petrov, V.; Mateos, X. et al. Passive Mode-Locking of a Tm-doped Bulk Laser Near 2  $\mu\text{m}$  using a Carbon Nanotube Saturable Absorber. *Opt. Express* **2009**, *17*, 11007–11012.
  10. Högele, A.; Galland, C.; Winger, M.; Imamoğlu, A. Photon Antibunching in the Photoluminescence Spectra of a Single Carbon Nanotube. *Phys. Rev. Lett.* **2008**, *100*, 217401.
  11. Cognet, L.; Tsyboulski, D.; Rocha, J.; Doyle, C.; Tour, J.; Weisman, R. Stepwise Quenching of Exciton Fluorescence in Carbon Nanotubes by Single-Molecule Reactions. *Science* **2007**, *316*, 1465.
  12. Rajan, A.; Strano, M. S.; Heller, D. A.; Hertel, T.; Schulten, K. Length-Dependent Optical Effects in Single Walled Carbon Nanotubes. *J. Phys. Chem. B* **2008**, *112*, 6211–6213.
  13. Hertel, T.; Himmelein, S.; Ackermann, T.; Stich, D.; Crochet, J. Diffusion Limited Photoluminescence Quantum Yields in 1-D Semiconductors: Single-Wall Carbon Nanotubes. *ACS Nano* **2010**, *4*, 7161–7168.
  14. Miyauchi, Y.; Matsuda, K.; Yamamoto, Y.; Nakashima, N.; Kanemitsu, Y. Length-Dependent Photoluminescence Lifetimes in Single-Walled Carbon Nanotubes. *J. Phys. Chem. C* **2010**, *114*, 12905–12908.
  15. Liu, T.; Xiao, Z. Exact and Closed Form Solutions for the Quantum Yield, Exciton Diffusion Length, and Lifetime To Reveal the Universal Behaviors of the Photoluminescence of Defective Single-Walled Carbon Nanotubes. *J. Phys. Chem. C* **2011**, *115*, 16920–16927.
  16. Harrah, D. M.; Swan, A. K. The Role of Length and Defects on Optical Quantum Efficiency and Exciton Decay Dynamics in Single-Walled Carbon Nanotubes. *ACS Nano* **2011**, *5*, 647–655.



17. Cherukuri, T. K.; Tsyboulski, D. A.; Weisman, R. B. Length- and Defect-Dependent Fluorescence Efficiencies of Individual Single-Walled Carbon Nanotubes. *ACS Nano* **2012**, *6*, 843–850.
18. Moritsubo, S.; Murai, T.; Shimada, T.; Murakami, Y.; Chiashi, S.; Maruyama, S.; Kato, Y. K. Exciton Diffusion in Air-Suspended Single-Walled Carbon Nanotubes. *Phys. Rev. Lett.* **2010**, *104*, 247402.
19. Siitonen, A. J.; Bachilo, S. M.; Tsyboulski, D. A.; Weisman, R. B. Evidence for Long-lived, Optically Generated Quenchers of Excitons in Single-Walled Carbon Nanotubes. *Nano Lett.* **2012**, *12*, 33–38.
20. Murakami, Y.; Kono, J. Nonlinear Photoluminescence Excitation Spectroscopy of Carbon Nanotubes: Exploring the Upper Density Limit of One-Dimensional Excitons. *Phys. Rev. Lett.* **2009**, *102*, 037401.
21. Xiao, Y.-F.; Nhan, T. Q.; Wilson, M. W. B.; Fraser, J. M. Saturation of the Photoluminescence at Few-Exciton Levels in a Single-Walled Carbon Nanotube under Ultrafast Excitation. *Phys. Rev. Lett.* **2010**, *104*, 017401.
22. Murakami, Y.; Kono, J. Existence of an Upper Limit on the Density of Excitons in Carbon Nanotubes by Diffusion-Limited Exciton-Exciton Annihilation: Experiment and Theory. *Phys. Rev. B* **2009**, *80*, 035432.
23. Srivastava, A.; Kono, J. Diffusion-Limited Exciton-Exciton Annihilation in Single-Walled Carbon Nanotubes: A Time-Dependent Analysis. *Phys. Rev. B* **2009**, *79*, 205407.
24. Karatzas, I.; Shreve, S. E. *Brownian Motion and Stochastic Calculus*, 2nd ed.; Springer: New York, New York, 1991.
25. Berciaud, S.; Cognet, L.; Lounis, B. Luminescence Decay and the Absorption Cross Section of Individual Single-Walled Carbon Nanotubes. *Phys. Rev. Lett.* **2008**, *101*, 077402.

26. Hagen, A.; Steiner, M.; Raschke, M.; Lienau, C.; Hertel, T.; Qian, H.; Meixner, A.; Hartschuh, A. Exponential Decay Lifetimes of Excitons in Individual Single-Walled Carbon Nanotubes. *Phys. Rev. Lett.* **2005**, *95*, 197401.
27. Lefebvre, J.; Finnie, P. Polarized Light Microscopy and Spectroscopy of Individual Single-Walled Carbon Nanotubes. *Nano Res.* **2011**, *4*, 788–794.
28. Lüer, L.; Hoseinkhani, S.; Polli, D.; Crochet, J.; Hertel, T.; Lanzani, G. Size and Mobility of Excitons in (6, 5) Carbon Nanotubes. *Nat. Phys.* **2008**, *5*, 54–58.
29. Siitonen, A. J.; Tsyboulski, D. A.; Bachilo, S. M.; Weisman, R. B. Surfactant-Dependent Exciton Mobility in Single-Walled Carbon Nanotubes Studied by Single-Molecule Reactions. *Nano Lett.* **2010**, *10*, 1595–1599.
30. Torney, D. C.; McConnell, H. M. Diffusion-limited Reactions in One Dimension. *J. Phys. Chem.* **1983**, *87*, 1941–1951.
31. Tonks, L. The Complete Equation of State of One, Two and Three-Dimensional Gases of Hard Elastic Spheres. *Phys. Rev.* **1936**, *50*, 955–963.
32. Miyauchi, Y.; Matsuda, K.; Kanemitsu, Y. Femtosecond excitation correlation spectroscopy of single-walled carbon nanotubes: Analysis based on nonradiative multiexciton recombination processes. *Phys. Rev. B* **2009**, *80*, 235433.
33. Joh, D. Y.; Kinder, J.; Herman, L. H.; Ju, S.-Y.; Segal, J. N., Michael A. Johnson; Chan, G. K.-L.; Park, J. Single-Walled Carbon Nanotubes as Excitonic Optical Wires. *Nat. Nanotechnol.* **2011**, *6*, 51–56.

This material is available free of charge via the Internet at <http://pubs.acs.org/>.